

# Electron-ion bremsstrahlung spectra calculations for sonoluminescence

Dominik Hammer and Lothar Frommhold

*Department of Physics, The University of Texas at Austin, Austin, Texas 78712*

(Received 20 June 2002; published 13 November 2002)

The bremsstrahlung spectra arising from electron-ion collisions are calculated for temperatures from 5000 K to 40 000 K and wavelengths from 100 nm to 1000 nm, for the ions He<sup>+</sup>, Ne<sup>+</sup>, Ar<sup>+</sup>, Kr<sup>+</sup>, Xe<sup>+</sup>, H<sup>+</sup>, and O<sup>+</sup>, using Hartree-Fock-Slater potentials. The spectral intensities are expressed in terms of Gaunt factors, the ratios of the present quantum computation and existing semiclassical results. For the heavy rare gas ions Gaunt factors of up to 3 are obtained at wavelengths of 200 nm. We use these results to improve our calculations of rare gas sonoluminescence spectra [Phys. Rev. E **65**, 046309 (2002)] and find that the improved overall sonoluminescence spectra hardly differ from our earlier results which were based on the semiclassical treatment of the electron-ion bremsstrahlung contributions. We think that in the conventional single-bubble sonoluminescence studies electron-ion bremsstrahlung amounts to but a small percentage of the overall emission. We also estimate here the effects of shielding of the ions due to a finite Debye length. Unless the Debye length is smaller than about 50 bohr, no significant influence of Debye shielding is discernible.

DOI: 10.1103/PhysRevE.66.056303

PACS number(s): 78.60.Mq, 41.60.-m, 52.25.Os

## I. INTRODUCTION

Early studies of sonoluminescence have considered electron-ion bremsstrahlung as one of the principal light-generating processes [1,2]. In more recent times theoretical evidence has emerged that electron-neutral bremsstrahlung is likely to be the principal radiative mechanism [3–9] of ordinary single-bubble sonoluminescence measurements, i.e., when bubbles are maintained over long periods of time. However, renewed interest in less stable, nonuniform bubble models with their higher core temperatures warrants a closer investigation of the electron-ion processes [8]. In addition, at the very high densities in the bubble also very high electron densities exist, even if the degree of ionization is small, which cause a Debye-type shielding of the ions. Effects of this process on the emission of radiation should also be taken into account.

## II. GAUNT FACTORS

In a semiclassical approximation the absorption coefficient  $\kappa_{\text{class}}^{e-i}(\lambda)$  for inverse bremsstrahlung of electron–singly charged ion scattering at wavelength  $\lambda$  and temperature  $T$  is given by [10]

$$\begin{aligned} \kappa_{\text{class}}^{e-i}(\lambda) = & \frac{4}{3} \left( \frac{2\pi}{3m_e k_B T} \right)^{1/2} \frac{e^6}{(4\pi\epsilon_0)^3 m_e^3 h c^4} n_e n \lambda^3 \\ & \times \left[ 1 - \exp \left( - \frac{hc}{\lambda k_B T} \right) \right]. \end{aligned} \quad (1)$$

In this expression, stimulated emission is taken into account;  $m_e$  is the mass and  $e$  the magnitude of the charge of the electron;  $n$  and  $n_e$  are the number densities of ions and electrons;  $\epsilon_0$  is the dielectric constant of vacuum;  $c$  is the speed of light; and  $k_B$  is Boltzmann's constant. The differences between this semiclassical result and quantum computations are commonly expressed by (temperature-averaged) Gaunt factors  $\xi(\lambda, T)$ ,

$$\kappa_{\text{quant}}^{e-i}(\lambda, T) = \xi(\lambda, T) \kappa_{\text{class}}^{e-i}(\lambda, T). \quad (2)$$

In the case of electron–hydrogen ion scattering the (not temperature averaged) Gaunt factor  $g(\epsilon, \epsilon')$  can be calculated exactly and is given by [11]

$$\begin{aligned} g(\epsilon, \epsilon') = & \frac{\pi\sqrt{3}}{(\sqrt{\epsilon'} - \sqrt{\epsilon})} \\ & \times \frac{|U(\epsilon, \epsilon')^2 - U(\epsilon', \epsilon)^2|}{[1 - \exp(-2\pi/\sqrt{\epsilon})][\exp(2\pi/\sqrt{\epsilon'}) - 1]}, \end{aligned} \quad (3)$$

where  $U(\epsilon, \epsilon')$  is given by a hypergeometric function

$$U(\epsilon, \epsilon') = {}_2F_1 \left( -\frac{i}{\sqrt{\epsilon}} + 1; -\frac{i}{\sqrt{\epsilon'}}; 1; \frac{-4\sqrt{\epsilon\epsilon'}}{(\sqrt{\epsilon'} - \sqrt{\epsilon})^2} \right). \quad (4)$$

Initial and final kinetic energies  $\epsilon$  and  $\epsilon'$  of the electron are measured in rydberg. Temperature averaging is done according to

$$\xi(\lambda, T) = \int_0^\infty g \left( \epsilon, \epsilon + \frac{hc}{\lambda} \right) \exp \left( - \frac{\epsilon}{k_B T} \right) \frac{d\epsilon}{k_B T}. \quad (5)$$

The thermally averaged Gaunt factors  $\xi(\lambda, T)$  for hydrogen we obtain in this way are given in Table I for wavelengths from 100 nm to 1000 nm and temperatures of 5, 10, 20, and 40 kK.

We account for the fact that a certain non-negligible electron density already exists that shields the ionic charge (Debye screening). If the interaction between electron and ion is given by a potential

$$V(r) = - \frac{Z(r)}{r}, \quad (6)$$

TABLE I. Exact Gaunt factors for hydrogen.

Wavelength (nm)	T (kK)			
	5	10	20	40
100	1.112	1.121	1.137	1.167
200	1.111	1.125	1.153	1.204
300	1.109	1.129	1.166	1.232
400	1.109	1.133	1.177	1.256
500	1.109	1.137	1.188	1.278
600	1.109	1.141	1.199	1.298
700	1.110	1.145	1.209	1.316
800	1.111	1.150	1.218	1.333
900	1.113	1.154	1.228	1.350
1000	1.114	1.158	1.236	1.365

where the  $r$  dependence of the ionic charge takes into account the inner structure of the ion, the Debye-screened interaction is [12]

$$V(r,d) = -\frac{Z(r) - [1 - \exp(-r/d)]}{r}, \quad (7)$$

where  $d$  is the Debye radius [13]

$$d(n_e, T) = \sqrt{\frac{\epsilon_0 k_B T}{2e^2 n_e}}. \quad (8)$$

To obtain the quantum mechanical Gaunt factors, we solve the Schrödinger equation for the scattering problem described by the potential  $V(r,d)$ , Eq. (7) above, for the initial and final scattering state and then use Fermi's golden rule to determine dipole matrix elements for the transition between those two continuum states.

### III. RESULTS

First we compute Gaunt factors  $\xi(\lambda, T)$  in this way for hydrogen [where  $Z(r)=1$ ] for Debye radii of  $12.5a_0$ ,  $25a_0$ ,  $50a_0$ ,  $100a_0$ , and  $200a_0$ , see Table II, where  $a_0$  denotes

Bohr's radius of the hydrogen atom. Comparing with the analytical calculation for  $d=\infty$  we see that for  $d=200a_0$  the two results agree within a few percent;  $d=200a_0$  is essentially equivalent to  $d=\infty$ . Also the results for  $d=200a_0$  and  $d=100a_0$  agree closely, while at  $d=12.5a_0$  the intensity is reduced by up to 30%. We furthermore notice that at short wavelengths the Debye shielding has the smallest effect while at long wavelengths the effect is the greatest. In a classical picture we can easily understand why this is the case. Long wavelengths are emitted principally in distant collisions that are affected most by Debye shielding, while emission at short wavelengths originates from the rapid accelerations close to the core region of the ion, where effects of the Debye screening should be less significant. Note that the shielding has similar effects at all temperatures, i.e., the intensity reduction due to increased shielding mostly depends on the wavelengths and hardly on the temperature. Our results agree qualitatively as well as quantitatively well with those published in Refs. [11,14], where similar situations were considered.

We proceed to compute the Gaunt factors for the rare gases and also for oxygen, for which no previous results seem to exist. To obtain the form  $Z(r)$  of the interaction potential, see Eqs. (6) and (7), we use the Hartree-Fock-Slater electron-ion interaction potentials given in Ref. [15]. Those are the same potentials that we applied to our previous computation of the electron-atom bremsstrahlung spectra [7,16]. Our results are given in Tables III–VIII. As in the case of hydrogen, the results for  $d=100a_0$  and  $d=200a_0$  agree to within a few per cent such that we can assume that again  $d=200a_0$  models well the situation for  $d=\infty$ . Again, as in the case of hydrogen, the Gaunt factors are reduced significantly with decreasing Debye radius, for xenon at  $d=12.5a_0$  to less than half that of  $d=200a_0$ .

In Ref. [12] the influence of Debye screening on electron-ion bremsstrahlung for argon was investigated as well and the small influence of the screening in the parameter range studied was noted, which agrees with our computations. However, in Ref. [12] Gaunt factors are also determined for the rare gases neon to xenon without Debye screening [17],

TABLE II. Gaunt factors for hydrogen.

Wave-length (nm)	$d (a_0)$																			
	12.5				25				50				100				200			
	5	10	20	40	5	10	20	40	5	10	20	40	5	10	20	40	5	10	20	40
100	1.059	1.064	1.078	1.108	1.077	1.090	1.109	1.140	1.101	1.109	1.125	1.156	1.106	1.115	1.131	1.161	1.109	1.117	1.134	1.164
200	0.990	1.009	1.038	1.088	1.053	1.072	1.103	1.155	1.089	1.104	1.132	1.183	1.100	1.115	1.143	1.194	1.105	1.120	1.148	1.198
300	0.933	0.961	1.001	1.064	1.032	1.056	1.096	1.162	1.078	1.098	1.136	1.203	1.095	1.115	1.152	1.218	1.102	1.121	1.159	1.225
400	0.883	0.918	0.965	1.038	1.013	1.041	1.088	1.166	1.069	1.094	1.140	1.219	1.090	1.115	1.160	1.240	1.100	1.124	1.169	1.248
500	0.842	0.882	0.935	1.014	0.996	1.028	1.081	1.168	1.062	1.091	1.143	1.233	1.087	1.116	1.168	1.258	1.098	1.126	1.178	1.268
600	0.804	0.848	0.905	0.990	0.980	1.015	1.073	1.168	1.056	1.088	1.146	1.245	1.085	1.117	1.175	1.275	1.097	1.129	1.188	1.287
700	0.769	0.816	0.878	0.967	0.965	1.003	1.066	1.166	1.050	1.086	1.149	1.256	1.083	1.118	1.182	1.291	1.097	1.132	1.196	1.304
800	0.738	0.788	0.853	0.946	0.951	0.991	1.058	1.163	1.045	1.083	1.152	1.265	1.081	1.120	1.189	1.305	1.097	1.135	1.205	1.320
900	0.708	0.761	0.829	0.926	0.938	0.980	1.050	1.159	1.040	1.081	1.154	1.273	1.079	1.121	1.195	1.318	1.097	1.138	1.213	1.335
1000	0.682	0.736	0.807	0.908	0.925	0.969	1.042	1.155	1.036	1.079	1.156	1.280	1.078	1.122	1.201	1.330	1.097	1.141	1.220	1.349

TABLE III. Gaunt factors for helium.

Wave-length (nm)	$d (a_0)$																			
	12.5				25				50				100				200			
									$T (\text{kK})$											
	5	10	20	40	5	10	20	40	5	10	20	40	5	10	20	40	5	10	20	40
100	1.303	1.329	1.374	1.457	1.370	1.395	1.440	1.522	1.408	1.430	1.472	1.552	1.422	1.444	1.487	1.566	1.429	1.451	1.493	1.572
200	1.030	1.067	1.127	1.231	1.134	1.167	1.224	1.328	1.185	1.213	1.269	1.371	1.205	1.233	1.288	1.390	1.214	1.242	1.297	1.399
300	0.922	0.967	1.034	1.149	1.055	1.092	1.156	1.273	1.115	1.148	1.211	1.327	1.139	1.172	1.234	1.351	1.150	1.182	1.245	1.361
400	0.855	0.904	0.977	1.099	1.013	1.053	1.123	1.249	1.082	1.118	1.188	1.315	1.109	1.146	1.216	1.343	1.122	1.159	1.228	1.355
500	0.808	0.860	0.937	1.063	0.985	1.028	1.103	1.236	1.062	1.102	1.177	1.314	1.094	1.133	1.209	1.345	1.108	1.147	1.223	1.359
600	0.768	0.823	0.903	1.032	0.964	1.009	1.089	1.227	1.050	1.092	1.172	1.316	1.084	1.127	1.207	1.352	1.100	1.142	1.223	1.367
700	0.733	0.791	0.873	1.005	0.946	0.993	1.077	1.220	1.040	1.085	1.170	1.320	1.078	1.123	1.209	1.361	1.095	1.140	1.226	1.378
800	0.703	0.762	0.846	0.981	0.931	0.980	1.066	1.213	1.033	1.080	1.169	1.325	1.073	1.122	1.212	1.371	1.092	1.140	1.230	1.389
900	0.675	0.736	0.822	0.960	0.917	0.967	1.056	1.206	1.027	1.076	1.169	1.330	1.070	1.121	1.215	1.380	1.090	1.141	1.235	1.401
1000	0.649	0.712	0.800	0.940	0.904	0.956	1.047	1.200	1.022	1.073	1.169	1.335	1.068	1.121	1.219	1.390	1.089	1.143	1.241	1.412

TABLE IV. Gaunt factors for neon.

Wave-length (nm)	$d (a_0)$																			
	12.5				25				50				100				200			
									$T (\text{kK})$											
	5	10	20	40	5	10	20	40	5	10	20	40	5	10	20	40	5	10	20	40
100	0.546	0.607	0.717	0.941	0.677	0.730	0.838	1.068	0.739	0.792	0.902	1.136	0.771	0.825	0.935	1.170	0.787	0.841	0.952	1.188
200	0.244	0.292	0.378	0.558	0.353	0.396	0.483	0.672	0.405	0.448	0.537	0.730	0.432	0.475	0.565	0.760	0.445	0.489	0.579	0.774
300	0.271	0.316	0.393	0.552	0.389	0.427	0.505	0.676	0.440	0.479	0.559	0.735	0.466	0.505	0.586	0.764	0.478	0.517	0.599	0.778
400	0.319	0.363	0.433	0.577	0.450	0.486	0.558	0.717	0.503	0.540	0.615	0.782	0.529	0.565	0.642	0.812	0.541	0.577	0.655	0.826
500	0.361	0.403	0.467	0.600	0.505	0.538	0.606	0.758	0.561	0.596	0.668	0.830	0.587	0.622	0.696	0.861	0.599	0.634	0.709	0.875
600	0.391	0.432	0.491	0.615	0.549	0.580	0.645	0.791	0.610	0.643	0.714	0.872	0.636	0.670	0.743	0.906	0.648	0.683	0.756	0.921
700	0.412	0.451	0.507	0.625	0.583	0.613	0.676	0.818	0.649	0.682	0.752	0.908	0.677	0.711	0.783	0.945	0.689	0.724	0.797	0.961
800	0.426	0.464	0.517	0.629	0.609	0.639	0.700	0.838	0.681	0.714	0.783	0.939	0.710	0.745	0.818	0.979	0.723	0.758	0.832	0.996
900	0.434	0.471	0.521	0.631	0.629	0.659	0.719	0.854	0.708	0.741	0.810	0.965	0.739	0.774	0.847	1.010	0.752	0.788	0.863	1.028
1000	0.438	0.474	0.523	0.630	0.645	0.674	0.733	0.866	0.730	0.763	0.833	0.987	0.762	0.798	0.873	1.037	0.777	0.813	0.889	1.056

TABLE V. Gaunt factors for argon.

Wave-length (nm)	$d (a_0)$																			
	12.5				25				50				100				200			
									$T (\text{kK})$											
	5	10	20	40	5	10	20	40	5	10	20	40	5	10	20	40	5	10	20	40
100	1.556	1.799	2.384	3.517	2.028	2.327	3.028	4.192	2.317	2.670	3.424	4.572	2.498	2.873	3.644	4.771	2.593	2.979	3.758	4.871
200	1.538	1.728	2.047	2.560	1.995	2.146	2.453	2.930	2.171	2.335	2.648	3.106	2.272	2.438	2.749	3.193	2.321	2.488	2.799	3.235
300	0.955	1.168	1.515	2.011	1.475	1.658	1.972	2.404	1.713	1.893	2.191	2.587	1.837	2.011	2.297	2.672	1.896	2.068	2.348	2.712
400	0.673	0.868	1.202	1.692	1.144	1.329	1.647	2.085	1.385	1.568	1.873	2.276	1.509	1.689	1.982	2.366	1.570	1.748	2.035	2.407
500	0.549	0.722	1.033	1.507	0.966	1.141	1.451	1.891	1.191	1.368	1.671	2.083	1.308	1.484	1.779	2.173	1.366	1.541	1.831	2.216
600	0.490	0.644	0.933	1.391	0.870	1.033	1.331	1.767	1.080	1.248	1.544	1.961	1.188	1.358	1.649	2.052	1.243	1.413	1.701	2.095
700	0.459	0.600	0.869	1.312	0.814	0.965	1.252	1.684	1.012	1.172	1.461	1.880	1.114	1.277	1.564	1.972	1.165	1.329	1.614	2.015
800	0.442	0.571	0.824	1.255	0.779	0.921	1.198	1.624	0.969	1.121	1.404	1.824	1.065	1.222	1.506	1.917	1.114	1.273	1.555	1.961
900	0.430	0.550	0.791	1.211	0.756	0.891	1.158	1.579	0.940	1.087	1.364	1.783	1.033	1.185	1.465	1.879	1.080	1.234	1.514	1.923
1000	0.421	0.534	0.764	1.177	0.740	0.868	1.128	1.545	0.921	1.062	1.335	1.754	1.011	1.159	1.435	1.852	1.057	1.207	1.484	1.896

TABLE VI. Gaunt factors for krypton.

Wave-length (nm)	$d(a_0)$																			
	12.5					25					50					100				
											$T$ (kK)									
	5	10	20	40		5	10	20	40		5	10	20		40	5	10	20	40	5
100	2.040	2.328	2.839	3.590	2.688	2.957	3.456	4.126	2.998	3.285	3.775	4.391	3.179	3.465	3.940	4.521	3.269	3.555	4.022	4.583
200	1.648	1.846	2.157	2.616	2.144	2.294	2.569	2.976	2.331	2.489	2.757	3.138	2.438	2.592	2.851	3.216	2.489	2.642	2.896	3.253
300	1.173	1.372	1.676	2.111	1.684	1.836	2.094	2.473	1.889	2.038	2.281	2.634	1.996	2.138	2.370	2.708	2.047	2.186	2.412	2.743
400	0.884	1.076	1.374	1.808	1.377	1.532	1.792	2.177	1.592	1.741	1.985	2.347	1.700	1.843	2.077	2.424	1.751	1.891	2.120	2.460
500	0.719	0.899	1.188	1.618	1.182	1.336	1.597	1.989	1.397	1.545	1.793	2.165	1.503	1.647	1.885	2.245	1.554	1.695	1.928	2.282
600	0.623	0.791	1.067	1.492	1.058	1.208	1.466	1.864	1.269	1.415	1.664	2.046	1.373	1.516	1.757	2.129	1.423	1.564	1.801	2.167
700	0.563	0.720	0.984	1.402	0.974	1.120	1.376	1.775	1.182	1.325	1.574	1.963	1.282	1.424	1.668	2.049	1.332	1.472	1.713	2.088
800	0.523	0.670	0.924	1.336	0.916	1.057	1.309	1.710	1.120	1.261	1.510	1.904	1.218	1.359	1.605	1.993	1.267	1.407	1.650	2.033
900	0.494	0.633	0.878	1.285	0.873	1.010	1.259	1.659	1.075	1.214	1.462	1.861	1.171	1.311	1.558	1.953	1.220	1.359	1.604	1.994
1000	0.472	0.604	0.841	1.244	0.840	0.974	1.219	1.620	1.041	1.178	1.426	1.827	1.136	1.275	1.523	1.923	1.184	1.323	1.569	1.966

TABLE VII. Gaunt factors for xenon.

Wave-length (nm)	$d(a_0)$																			
	12.5					25					50					100				
											$T$ (kK)									
	5	10	20	40		5	10	20	40		5	10	20		40	5	10	20	40	5
100	2.116	2.827	3.962	5.870	3.871	4.477	5.410	7.127	4.778	5.269	6.077	7.725	5.172	5.612	6.372	8.007	5.357	5.770	6.509	8.141
200	1.900	2.080	2.190	2.576	2.477	2.475	2.423	2.818	2.617	2.525	2.433	2.895	2.631	2.500	2.408	2.924	2.624	2.475	2.389	2.936
300	1.644	1.837	2.028	2.315	2.199	2.290	2.364	2.588	2.388	2.438	2.466	2.685	2.455	2.488	2.497	2.721	2.483	2.507	2.508	2.736
400	1.395	1.575	1.780	2.071	1.913	2.008	2.128	2.362	2.092	2.160	2.250	2.475	2.158	2.217	2.296	2.520	2.187	2.241	2.315	2.539
500	1.200	1.372	1.582	1.883	1.699	1.797	1.937	2.190	1.876	1.952	2.070	2.315	1.943	2.012	2.123	2.366	1.972	2.038	2.146	2.388
600	1.048	1.215	1.429	1.740	1.533	1.634	1.789	2.060	1.713	1.795	1.933	2.197	1.782	1.859	1.991	2.255	1.814	1.888	2.017	2.280
700	0.930	1.093	1.309	1.630	1.402	1.508	1.673	1.959	1.587	1.676	1.828	2.110	1.660	1.744	1.892	2.173	1.693	1.775	1.921	2.201
800	0.837	0.997	1.215	1.543	1.298	1.407	1.582	1.881	1.489	1.582	1.746	2.043	1.564	1.655	1.815	2.112	1.600	1.688	1.847	2.142
900	0.764	0.920	1.139	1.473	1.214	1.326	1.508	1.817	1.410	1.508	1.681	1.990	1.488	1.584	1.756	2.065	1.526	1.620	1.789	2.098
1000	0.704	0.857	1.076	1.416	1.145	1.259	1.448	1.765	1.345	1.448	1.629	1.949	1.427	1.528	1.708	2.029	1.467	1.565	1.744	2.064

TABLE VIII. Gaunt factors for oxygen.

Wave-length (nm)	$d(a_0)$																			
	12.5					25					50					100				
											$T$ (kK)									
	5	10	20	40		5	10	20	40		5	10	20		40	5	10	20	40	5
100	1.156	1.251	1.409	1.716	1.366	1.439	1.588	1.895	1.450	1.526	1.677	1.986	1.498	1.572	1.723	2.033	1.520	1.594	1.746	2.057
200	0.382	0.452	0.581	0.844	0.539	0.602	0.731	1.003	0.614	0.678	0.809	1.086	0.654	0.718	0.850	1.128	0.673	0.738	0.870	1.149
300	0.292	0.357	0.472	0.709	0.446	0.503	0.621	0.871	0.518	0.576	0.696	0.953	0.555	0.614	0.735	0.994	0.573	0.632	0.754	1.014
400	0.296	0.357	0.463	0.681	0.456	0.510	0.619	0.854	0.528	0.583	0.696	0.940	0.564	0.619	0.734	0.981	0.581	0.637	0.752	1.001
500	0.320	0.378	0.475	0.678	0.488	0.538	0.640	0.865	0.561	0.612	0.720	0.956	0.596	0.648	0.758	0.998	0.613	0.665	0.776	1.018
600	0.343	0.397	0.487	0.680	0.520	0.567	0.664	0.881	0.595	0.645	0.749	0.979	0.630	0.681	0.788	1.024	0.647	0.698	0.806	1.043
700	0.361	0.413	0.497	0.680	0.548	0.593	0.687	0.896	0.627	0.675	0.777	1.003	0.663	0.712	0.817	1.050	0.679	0.729	0.835	1.070
800	0.375	0.424	0.504	0.680	0.572	0.615	0.705	0.910	0.655	0.702	0.802	1.026	0.691	0.740	0.844	1.075	0.708	0.758	0.863	1.097
900	0.384	0.432	0.508	0.678	0.591	0.632	0.720	0.921	0.679	0.725	0.824	1.046	0.716	0.765	0.869	1.099	0.734	0.783	0.889	1.122
1000	0.391	0.436	0.509	0.675	0.606	0.647	0.733	0.929	0.700	0.745	0.844	1.064	0.738	0.787	0.891	1.121	0.757	0.806	0.912	1.145

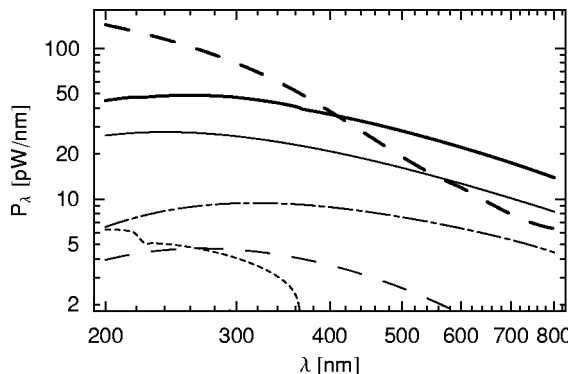


FIG. 1. Single bubble sonoluminescence (SBSL) spectrum and its composition for argon bubbles in water at freezing temperature. An SBSL bubble of ambient radius  $5.5 \mu\text{m}$ , driven at an ultrasound frequency of  $33.4 \text{ kHz}$  with an amplitude of  $1.48 \text{ bar}$ , was assumed. Shown are the total spectrum (thick solid line) and contributions due to electron-neutral argon bremsstrahlung (thin solid line),  $\text{O}^-$  radiation (dotted line),  $\text{H}^-$  radiation (dashed line), and  $e\text{-Ar}^+$  bremsstrahlung (dash-dotted line). For comparison, the measured spectrum is indicated by the thick dashed line [2,21].

which should be comparable to our results for the largest  $d = 200a_0$  of our work. Indeed, for neon the two computations agree within a few percent. However, for the heavier rare gases substantial differences are observed, with the values in Ref. [17] being larger than ours by up to a factor of two at short wavelengths. The differences between these computations increase with decreasing wavelengths, the reason being the different choices of the electron-ion interaction potential. Instead of the Hartree-Fock-Slater potential we use, in Ref. [17] a scaled Thomas-Fermi potential was used; see Ref. [18], where the scaled Thomas-Fermi potential is described and compared with the Hartree-Fock-Slater potentials. Indeed, repeating our computations with scaled Thomas-Fermi potentials [17] shows agreement. It is not obvious which of the two approximations of the electron-ion interaction is more realistic [18]. We continue to use the Hartree-Fock-Slater potentials for consistency with our earlier computations of electron-atom bremsstrahlung [7,16]. We regard the differences of the computations with Hartree-Fock-Slater and the scaled Thomas-Fermi potentials as the uncertainty of the theoretical results [12,17].

Figure 1 shows a spectrum computed from our current model of sonoluminescence for argon bubbles in freezing water. For the experimental parameters the same values were

chosen as in Ref. [8] so that the computations are directly comparable, see especially Fig. 1 of Ref. [8]. To illustrate the maximum effect of taking the quantum effects of electron-ion bremsstrahlung into account, relative to the computations shown in Ref. [8], we repeated the calculation in which electron-ion bremsstrahlung has the largest relative contribution. Furthermore, instead of the smaller values for the Gaunt factor for argon computed in the present paper, we used the larger values given in Ref. [17]. Nevertheless, because of the relatively small significance of electron-ion bremsstrahlung, the difference in the total emitted intensity between the present computation and the earlier one with all Gaunt factors equal to unity is rather small, roughly 10%. This difference would be even smaller if we used the present Gaunt factors and especially if we included the effects of Debye screening in the computation since at the high densities in the sonoluminescing environment at the time of light emission the Debye radius can be as small as  $d = 20a_0$ . However, whereas in our current models of sonoluminescence it seems unnecessary to use Gaunt factors different from unity for electron-ion bremsstrahlung, we expect the situation to change in future work. Currently we use a model in which the entire bubble is assumed to be uniform. However, a refinement of theoretical modeling to nonuniform bubble models seems inescapable, with higher local temperatures and thus higher electron-ion bremsstrahlung contributions, as this is also indicated by the discrepancy of computed and observed total emitted spectrum in Fig. 1; see the discussion in Ref. [8].

#### IV. CONCLUSION

We have computed Gaunt factors for electron-ion bremsstrahlung for various atomic ions and conditions of interest in sonoluminescence. Additionally, we take into account the effects of Debye screening which turn out to be significant for Debye radii smaller than about  $50 a_0$ . While in our current model of sonoluminescence the corrections presented here seem to be insignificant, we expect this situation to change in more elaborate computations of the sonoluminescence continua.

#### ACKNOWLEDGMENT

The support of the R. A. Welch Foundation, Grant No. 1346, is gratefully acknowledged.

- 
- [1] C.C. Wu and P.H. Roberts, Proc. R. Soc. London, Ser. A **445**, 323 (1994).
  - [2] B.P. Barber *et al.*, Phys. Rep. **281**, 65 (1997).
  - [3] S. Hilgenfeldt, S. Grossmann, and D. Lohse, Nature (London) **398**, 402 (1999).
  - [4] S. Hilgenfeldt, S. Grossmann, and D. Lohse, Phys. Fluids **11**, 1318 (1999).
  - [5] D. Hammer and L. Frommhold, Phys. Fluids **12**, 472 (2000).
  - [6] D. Hammer and L. Frommhold, Phys. Rev. Lett. **85**, 1326 (2000).
  - [7] D. Hammer and L. Frommhold, J. Mod. Opt. **48**, 239 (2001).
  - [8] D. Hammer and L. Frommhold, Phys. Rev. E **65**, 046309 (2002).
  - [9] M.P. Brenner, S. Hilgenfeldt, and D. Lohse, Rev. Mod. Phys. **74**, 425 (2002).
  - [10] Y.B. Zel'dovich and Y.P. Raizer, *Physics of Shock Waves and High Temperature Hydrodynamic Phenomena* (Academic Press, New York, 1966), Vol. 1.

- [11] R. Lange and D. Schluter, J. Quant. Spectrosc. Radiat. Transf. **33**, 237 (1985).
- [12] R. Lange and D. Schluter, J. Quant. Spectrosc. Radiat. Transf. **48**, 153 (1992).
- [13] H. Griem, *Principles of Plasma Spectroscopy* (Cambridge University Press, New York, 1997).
- [14] R. Lange and D. Schluter, J. Quant. Spectrosc. Radiat. Transf. **35**, 237 (1986).
- [15] F. Herman and S. Skillman, *Atomic Structure Calculations* (Prentice-Hall, Englewood Cliffs, NJ, 1963).
- [16] L. Frommhold, Phys. Rev. E **58**, 1899 (1998).
- [17] D. Schluter, Z. Phys. D: At., Mol. Clusters **6**, 249 (1987).
- [18] J.C. Stewart and M. Rotenberg, Phys. Rev. **140**, A1508 (1965).
- [19] K.R. Weninger, C.G. Camara, and S.J. Putterman, Phys. Rev. E **63**, 016310 (2001).
- [20] G. Vazquez, C. Camara, S. Putterman, and K. Weninger, Opt. Lett. **26**, 575 (2001).
- [21] We divided the intensity of the experimental spectra by  $4\pi$  since this factor was reported to be missing in plots of the measured spectral intensity [19,20].